

# Chapter 2

## Study of Soil-Structure Interaction Problems Using Mixed FEM-BEM Formulations

Dimas Betioli Ribeiro and João Batista de Paiva

**Abstract** The objective of this paper is to present formulations developed for soil-building interaction analysis, including foundations. The soil is modeled with the boundary element method (BEM) as a layered solid which may be finite for the vertical direction, but is always infinite for radial directions. Infinite boundary elements are employed for the far field simulation, allowing computational cost reduction without compromising the result accuracy. Beams, columns and piles are modeled with the finite element method (FEM) using one dimensional elements. Slabs and rafts are also modeled with the FEM, but with two dimensional elements. The analysis is static and all materials are considered homogeneous, isotropic, elastic and with linear behavior.

**Keywords** Boundary elements • Finite elements • Soil-structure interaction • Pile • Raft • Slab

### 1 Introduction

The construction of buildings involve complex soil-structure interaction effects that require previous studies to be correctly considered in the project. The basis of these studies has to be chosen among many options available and each one of them implies on advantages and disadvantages, as described below.

When possible, a good choice is to employ analytical methods. When correctly programmed they give trustful results in little processing time. In Ref. [2], for example, a solution is presented for an axially loaded pile with a rectangular cross section and immersed in a layered isotropic domain. The main disadvantage of

---

D.B. Ribeiro (✉)

Federal Institute of Education, Science and Technology of São Paulo, Rua Antonio Fogaça de Almeida, s/n, Jardim Elza Maria, Jacareí, SP, Brazil  
e-mail: [dimasbetioli@gmail.com](mailto:dimasbetioli@gmail.com)

J.B. de Paiva

Department of Structural Engineering, School of Engineering of São Carlos, University of São Paulo, Av. Trabalhador Sãocarlense, 400, São Carlos, SP, Brazil  
e-mail: [paiva@sc.usp.br](mailto:paiva@sc.usp.br)

these solutions is that they suit only specific situations, so many researches keep developing new ones to include new problems. Another reference that may be cited is [9].

If analytical solutions cannot be used, one alternative would be a numerical approach. The developments [6] of the numerical methods in the latter years and its versatility made them attractive to many researchers. The finite element method (FEM) is still popular [5, 16], however has some disadvantages when compared to other options such as the boundary element method (BEM). The FEM require the discretization of the domain, which has to be simulated as infinite in most soil-structure interaction problems. This implies on a high number of elements, leading to a large and sometimes impracticable processing time.

It becomes more viable solving these problems with the BEM, once only the boundary of the domains involved is discretized. This allows reducing the problem dimension, implying on less processing time. This advantage is explored in several works [1, 7, 12] and new developments are making the BEM even more attractive to future applications. One is simulating non-homogeneous domains using an alternative multi-domain BEM technique [13], another is using mapping functions to make boundary elements infinite [14].

The objective of this paper is to present a formulation for building-soil interaction analysis that uses recent developments accomplished by the authors in Refs. [13–15]. The proposed formulation is applied into two examples. In the first, a squared raft resting on an infinite layered domain is considered. Results are compared with other formulations available in the literature including an analytical approach and good agreement is observed. The objective of the second example is to show all functionalities of the proposed formulation, considering a complete building interacting with a layered soil. No comparison with other authors is presented, nevertheless the results obtained may be considered coherent. Finally, it is concluded that the presented formulation may be considered a practical and attractive alternative in the field of soil-structure interaction simulation.

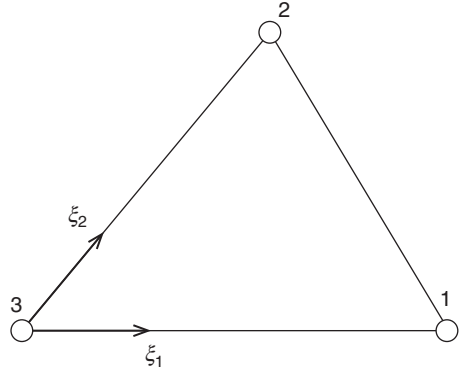
## 2 Boundary Element Formulation

The equilibrium of a solid body can be represented by a boundary integral equation called the Somigliana Identity, which for homogeneous, isotropic and linear-elastic domains is

$$c_{ij}(y) u_j(y) + \int_{\Gamma} p_{ij}^*(x, y) u_j(x) d\Gamma(x) = \int_{\Gamma} u_{ij}^*(x, y) p_j(x) d\Gamma(x) \quad (2.1)$$

Equation 2.1 is written for a source point  $y$  at the boundary, where the displacement is  $u_j(y)$ . The constant  $c_{ij}$  depends on the Poisson ratio and the boundary geometry at  $y$ , as pointed out in Ref. [11]. The field point  $x$  goes through the whole

**Fig. 2.1** Triangular boundary element



boundary  $\Gamma$ , where displacements are  $u_j(x)$  and tractions are  $p_j(x)$ . The integral kernels  $u_{ij}^*(x, y)$  and  $p_{ij}^*(x, y)$  are Kelvin three-dimensional fundamental solutions for displacements and tractions, respectively. Kernel  $u_{ij}^*(x, y)$  has order  $1/r$  and kernel  $p_{ij}^*(x, y)$  order  $1/r^2$ , where  $r = |x - y|$ , so the integrals have singularity problems when  $x$  approaches  $y$ . Therefore the stronger singular integral, over the traction kernel, has to be defined in terms of a Cauchy Principal Value (CPV).

To solve Eq. 2.1 numerically, the boundary is divided into regions within which displacements and tractions are approximated by known shape functions. Here these regions are of two types, finite boundary elements (BEs) and infinite boundary elements (IBEs). The BEs employed are triangular, as shown in Fig. 2.1 with the local system of coordinates,  $\xi_1\xi_2$ , and the local node numbering. The following approximations are used for this BE:

$$u_j = \sum_{k=1}^3 N^k u_j^k, \quad p_j = \sum_{k=1}^3 N^k p_j^k \quad (2.2)$$

Equation 2.2 relates the boundary values  $u_j$  and  $p_j$  to the nodal values of the BE. The BEs have 3 nodes and for each node there are three components of displacement  $u_j^k$  and traction  $p_j^k$ . The shape functions  $N^k$  used for these approximations are

$$N^1 = \xi_1, \quad N^2 = \xi_2, \quad N^3 = 1 - \xi_1 - \xi_2 \quad (2.3)$$

The same shape functions are used to approximate the boundary geometry and to interpolate displacements and tractions for the IBEs. The IBE geometry, on the other hand, is approximated by special mapping functions, as discussed in more detail in Sect. 3. By substituting Eq. 2.2 in 2.1, Eq. 2.4 is obtained:

$$c_{ij}u_j + \sum_{e=1}^{N_{BE}} \left\{ \sum_{k=1}^3 \left[ \Delta p_{ij}^{ek} u_j^k \right] \right\} + \sum_{e=1}^{N_{IBE}} \left\{ \sum_{k=1}^{N_p} \left[ \Delta^\infty p_{ij}^{ek} u_j^k \right] \right\}$$

$$= \sum_{e=1}^{N_{BE}} \left\{ \sum_{k=1}^3 \left[ \Delta u_{ij}^{ek} p_j^k \right] \right\} + \sum_{e=1}^{N_{IBE}} \left\{ \sum_{k=1}^{N_p} \left[ \Delta^\infty u_{ij}^{ek} p_j^k \right] \right\} \quad (2.4)$$

$N_{BE}$  is the number of BEs and  $N_{IBE}$  is the number of IBEs. For BEs:

$$\Delta p_{ij}^{ek} = \int_{\gamma_e} |J| N^k p_{ij}^* (x, y) d\gamma_e, \quad \Delta u_{ij}^{ek} = \int_{\gamma_e} |J| N^k u_{ij}^* (x, y) d\gamma_e \quad (2.5)$$

In Eq. 2.5,  $\gamma_e$  represents the domain of element  $e$  in the local coordinate system and the global system of coordinates is transformed to the local one by the Jacobian  $|J| = 2A$ , where  $A$  is the element area in the global system. On the other hand, for IBEs:

$$\Delta^\infty p_{ij}^{ek} = \int_{\gamma_e} |\infty J| N^k p_{ij}^* (x, y) d\gamma_e, \quad \Delta^\infty u_{ij}^{ek} = \int_{\gamma_e} |\infty J| N^k u_{ij}^* (x, y) d\gamma_e \quad (2.6)$$

Equation 2.6 is analogous to 2.5. Integrals of Eqs. 2.5 and 2.6 are calculated by standard BEM techniques. Non-singular integrals are evaluated numerically by using integration points. The singular ones, on the other hand, are evaluated by the technique presented in Ref. [10]. Finally, the free term  $c_{ij}$  may be obtained by rigid body motions. Writing Eq. 2.4 for all boundary nodes leads to

$$\Delta p \cdot u = \Delta u \cdot p \quad (2.7)$$

### 3 Infinite Boundary Elements

Three types of mapping are considered, as illustrated in Fig. 2.2.

In the first type, represented in Fig. 2.2a, only direction  $\xi_1$  is mapped to infinity and node 1 is placed at infinity. The IBE is represented in the local coordinate system on the left and in the global coordinate system on the right. The global coordinates  $x_i$  are related to the local ones by special mapping functions,  $M^k$ , and the nodal global coordinates,  $x_i^k$ . Node 4 is created only to replace node 1 in the mapping and does not contribute to the integrals.

Figure 2.2b is analogous to Fig. 2.2a, but in this case only direction  $\xi_2$  is mapped to infinity and node 2 is placed at infinity. Therefore, node 5 is created to facilitate the mapping. Finally, in Fig. 2.2c both local directions are mapped to infinity and nodes 1 and 2 are placed at infinity. As a result, the auxiliary nodes 4 and 5 must be created to replace them in the mapping.

In Ref. [14], auxiliary coordinates  $\bar{\xi}_1$  and  $\bar{\xi}_2$  are used to obtain the mapping functions for each case. When only direction  $\xi_1$  is mapped to infinity, the result is:

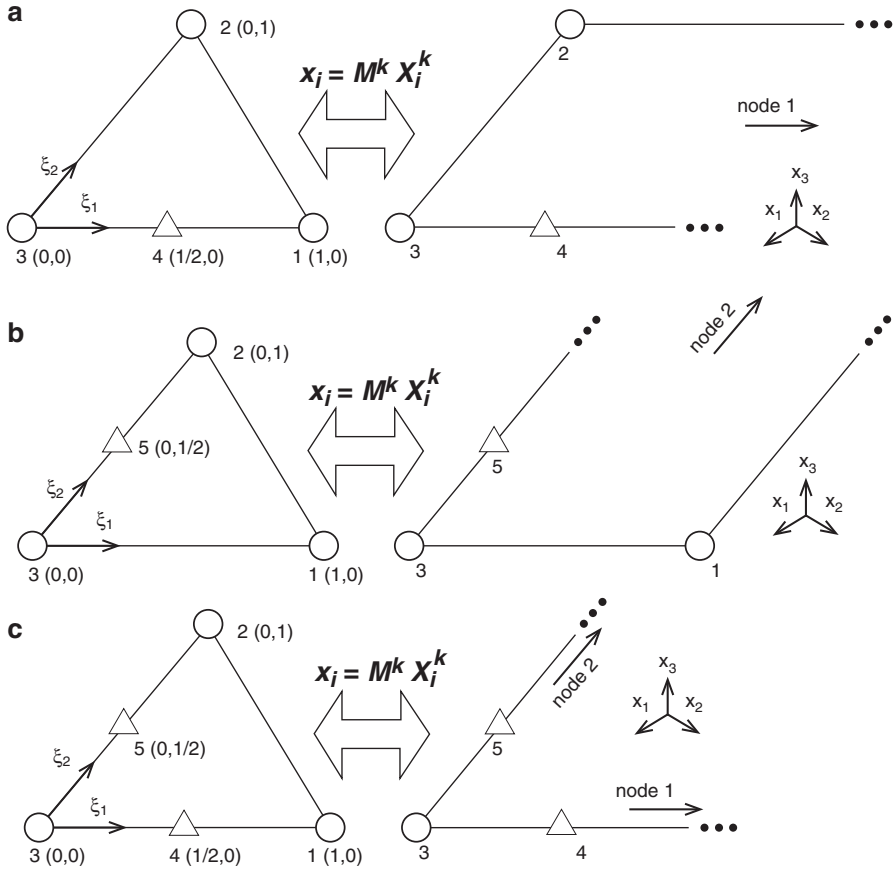


**Fig. 2.2** Types of mapping: (a) node 1 to infinity, (b) node 2 to infinity, (c) nodes 1 and 2 to infinity

$$M_{1\infty}^4 = \bar{\xi}_1(\xi_1) = \frac{\xi_1}{1 - \xi_1}, \quad M_{1\infty}^2 = \xi_2, \quad M_{1\infty}^3 = 1 - \bar{\xi}_1(\xi_1) - \xi_2 = 1 - \frac{\xi_1}{1 - \xi_1} - \xi_2 \quad (2.8)$$

The symbol “ $1\infty$ ” is used to indicate that these expressions are valid if only direction  $\xi_1$  is mapped to infinity. These functions are then employed to relate the local system of coordinates to the global one. In other words:

$$x_i = M_{1\infty}^4 x_i^4 + M_{1\infty}^2 x_i^2 + M_{1\infty}^3 x_i^3 \quad (2.9)$$

After obtaining Eq. 2.9, the Jacobian used when only direction  $\xi_1$  is mapped to infinity may be calculated as follows:

$$|^\infty J_1| = \frac{\partial x_1}{\partial \xi_1} \frac{\partial x_2}{\partial \xi_2} - \frac{\partial x_2}{\partial \xi_1} \frac{\partial x_1}{\partial \xi_2} = \frac{2A_1}{(1 - \xi_1)^2} \quad (2.10)$$

where  $A_1$  is the area of the triangle drawn between nodes 2, 3 and 4 in the global system of coordinates.

For mapping only in direction  $\xi_2$  to infinity, the functions obtained are:

$$M_{2\infty}^1 = \xi_1, \quad M_{2\infty}^5 = \bar{\xi}_2(\xi_2) = \frac{\xi_2}{1 - \xi_2}, \quad M_{2\infty}^3 = 1 - \xi_1 - \bar{\xi}_2(\xi_2) = 1 - \xi_1 - \frac{\xi_2}{1 - \xi_2} \quad (2.11)$$

The symbol “ $2\infty$ ” is used to indicate that only direction  $\xi_2$  is mapped to infinity. Therefore, the global system is related to the local one as follows:

$$x_i = M_{2\infty}^1 x_i^1 + M_{2\infty}^5 x_i^5 + M_{2\infty}^3 x_i^3 \quad (2.12)$$

and the Jacobian is

$$|^\infty J_2| = \frac{2A_2}{(1 - \xi_2)^2} \quad (2.13)$$

where  $A_2$  refers to the area of the triangle drawn between nodes 1, 3 and 5 in the global system of coordinates.

Finally, for mapping in both directions  $\xi_1$  and  $\xi_2$  to infinity, the mapping functions are

$$M_\infty^4 = \frac{\xi_1}{1 - \xi_1}, \quad M_\infty^5 = \frac{\xi_2}{1 - \xi_2}, \quad M_\infty^3 = 1 - \frac{\xi_1}{1 - \xi_1} - \frac{\xi_2}{1 - \xi_2} \quad (2.14)$$

The symbol “ $\infty$ ” is used to indicate that both directions are mapped to infinity. The local system of coordinates is related to the global one as follows:

$$x_i = M_\infty^4 x_i^4 + M_\infty^5 x_i^5 + M_\infty^3 x_i^3 \quad (2.15)$$

and the Jacobian is now

$$|^\infty J_3| = \frac{2A_3}{(1 - \xi_1)^2 (1 - \xi_2)^2} \quad (2.16)$$

where  $A_3$  is the area of the triangle drawn between nodes 3, 4 and 5 in the global system.

## 4 Load Lines in the Soil

In this work, the reactive tractions from the piles are applied in the soil as load lines. Figure 2.3 presents the model adopted, with four nodes equally spaced along the pile. The load lines influence may be computed in Eq. 2.1 with an additional term:

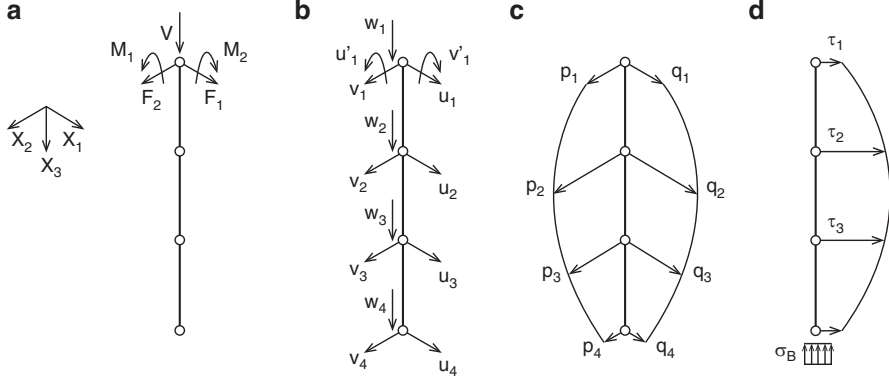


**Fig. 2.3** Model for load lines: (a) possible loads at the top node, (b) degrees of freedom, (c) horizontal tractions, (d) vertical tractions

$$c_{ij}(y)u_j(y) + \int_{\Gamma} p_{ij}^*(x, y)u_j(x) d\Gamma(x) = \int_{\Gamma} u_{ij}^*(x, y)p_j(x) d\Gamma(x) + \sum_{e=1}^{nl} \left[ \int_{\Gamma^e} u_{ij}^*(x, y)s_j^e(x) d\Gamma^e(x) \right] \quad (2.17)$$

where  $nl$  is the number of load lines,  $\Gamma^e$  are their external surface and  $s_j^e$  are the tractions presented in Fig. 2.3c, d. The tractions are approximated from the nodal values  $s_j^{ek}$  using  $nf$  polynomial shape functions  $\phi$ :

$$s_j^e = \sum_{k=1}^{nf} \phi^k s_j^{ek} \quad (2.18)$$

Shape functions are written with a dimensionless coordinate  $\xi = 2x_3/L - 1$ , where  $L$  is the load line length and  $x_3$  is the vertical global coordinate. For the horizontal tractions, illustrated in Fig. 2.3c,  $nf = 4$  and the shape functions are:

$$\begin{aligned} \phi^1 &= \frac{1}{16} (-9\xi^3 + 9\xi^2 + \xi - 1), & \phi^2 &= \frac{1}{16} (27\xi^3 - 9\xi^2 - 27\xi + 9), \\ \phi^3 &= \frac{1}{16} (-27\xi^3 - 9\xi^2 + 27\xi + 9), & \phi^4 &= \frac{1}{16} (9\xi^3 + 9\xi^2 - \xi - 1) \end{aligned} \quad (2.19)$$

For shear tractions in direction  $x_3$ ,  $nf = 3$  and the shape functions are

$$\phi^1 = \frac{1}{8} (9\xi^2 - 1), \quad \phi^2 = \frac{1}{4} (-9\xi^2 - 6\xi + 3), \quad \phi^3 = \frac{1}{8} (9\xi^2 + 12\xi + 3) \quad (2.20)$$

Finally, for the base reaction  $nf = 1$  and a constant approximation is used. The integrals that are not singular may be numerically calculated using Gauss points, while singular ones are analytically evaluated. Writing Eq. 2.20 for all boundary points plus the points defined on each load line, it is obtained:

$$[H] \{u\} = [G] \{p\} + [M] \{s\} \quad (2.21)$$

Matrix  $[M]$  is obtained from the integrals calculated for all load lines, and vector  $\{s\}$  contains the tractions prescribed for them. As the number of equations is equal to the number of unknowns, the system may be solved obtaining all unknowns.

## 5 FEM-BEM Coupling

Each pile is modeled using a single finite element with polynomial shape functions. Lateral displacements are approximated using fourth degree polynomials  $\{\varphi\}$ . Vertical displacements and lateral tractions are approximated using third degree polynomials  $\{\phi\}$ . Vertical tractions are approximated using second degree polynomials  $\{\omega\}$  and the tractions at the pile base are considered constant. Using a dimensionless coordinate  $\xi = \frac{x_3}{L}$ , where  $x_3$  is the global vertical coordinate and  $L$  is the pile length,  $\{\varphi\}$ ,  $\{\phi\}$  and  $\{\omega\}$  may be written as:

$$\begin{aligned} \{\varphi\} &= \begin{Bmatrix} -\frac{99}{4}\xi^4 + 45\xi^3 - \frac{85}{4}\xi^2 + 1 \\ -\frac{9}{2}\xi^4 L + 9\xi^3 L - \frac{11}{2}\xi^2 L + \xi L \\ \frac{81}{2}\xi^4 - \frac{135}{2}\xi^3 + 27\xi^2 \\ -\frac{81}{4}\xi^4 + 27\xi^3 - \frac{27}{4}\xi^2 \\ \frac{9}{2}\xi^4 - \frac{9}{2}\xi^3 + \xi^2 \end{Bmatrix}, \quad \{\phi\} = \begin{Bmatrix} -\frac{9}{2}\xi^3 + 9\xi^2 - \frac{11}{2}\xi + 1 \\ \frac{27}{2}\xi^3 - \frac{45}{2}\xi^2 + 9\xi \\ -\frac{27}{2}\xi^3 + 18\xi^2 - \frac{9}{2}\xi \\ \frac{9}{2}\xi^3 - \frac{9}{2}\xi^2 + \xi \end{Bmatrix}, \\ \{\omega\} &= \begin{Bmatrix} \frac{9}{2}\xi^2 - \frac{9}{2}\xi + 1 \\ -9\xi^2 + 6\xi \\ \frac{9}{2}\xi^2 - \frac{3}{2}\xi \end{Bmatrix} \end{aligned} \quad (2.22)$$

The next step is obtaining the total potential energy function, considering internal and external contributions. To obtain the final system of equations, such function must be minimized with respect to the nodal parameters. The result is:

$$[K] \{u\} = \{f\} - [Q] \{y\} \rightarrow [K] \{u\} = \{f\} - \{r\} \quad (2.23)$$



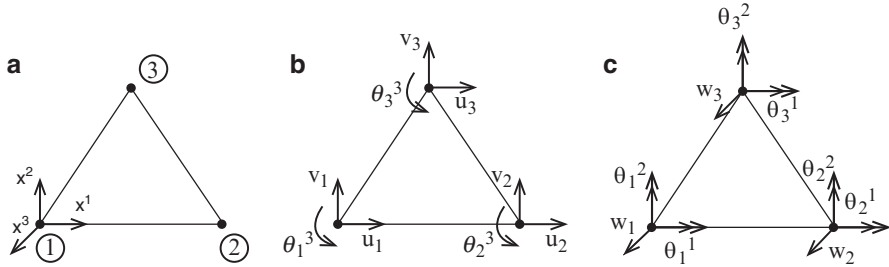


**Fig. 2.4** Triangular finite element: (a) local node numbering, (b) in plane degrees of freedom, (c) out of plane degrees of freedom

where  $[K]$  is the stiffness matrix of the pile,  $\{u\}$  contains nodal displacements,  $\{f\}$  contains nodal loads,  $\{y\}$  contains distributed tractions and  $[Q]$  is a matrix that transforms distributed tractions into nodal loads. Therefore,  $\{r\}$  contains nodal loads that represent the distributed loads.

Now a brief description of the triangular finite element used for the raft and slabs will be presented. The element has three nodes at its vertices as presented in Fig. 2.4a with the local node numbering and a local rectangular system of coordinates  $x^i$ , where the superscript  $i$  indicates the direction. Each node, indicated with the subscript  $j$ , has six degrees of freedom (DOFs). Three of them,  $u_j$ ,  $v_j$  and  $\theta_j^3$ , may be visualized in Fig. 2.4b which refers to the membrane effects. The other three,  $w_j$ ,  $\theta_j^1$  and  $\theta_j^2$ , are presented in Fig. 2.4c which refers to the plate effects. In Fig. 2.4c, rotational DOFs are indicated with a double arrow for better visualization. All DOFs of the finite element may be arranged into three vectors, as shown below:

$$\begin{aligned} \{\mathbf{u}_1\}^T &= \{u_1 \ v_1 \ \theta_1^3 \ w_1 \ \theta_1^1 \ \theta_1^2\}, \quad \{\mathbf{u}_2\}^T = \{u_2 \ v_2 \ \theta_2^3 \ w_2 \ \theta_2^1 \ \theta_2^2\}, \\ \{\mathbf{u}_3\}^T &= \{u_3 \ v_3 \ \theta_3^3 \ w_3 \ \theta_3^1 \ \theta_3^2\} \end{aligned} \quad (2.24)$$

Displacements at any point  $P$  of the finite element, with coordinates  $x_1$ ,  $x_2$  and  $x_3$ , may be written as

$$\{\mathbf{u}\} = \begin{Bmatrix} u \\ v \\ w \end{Bmatrix} = \begin{Bmatrix} u_0 - x_3 \frac{\partial w_0}{\partial x_1} \\ v_0 - x_3 \frac{\partial w_0}{\partial x_2} \\ w_0 \end{Bmatrix} \quad (2.25)$$

where  $u_0$ ,  $v_0$ , and  $w_0$  are the displacements for the projection of  $P$  at the mid plane of the finite element. The strain field may be obtained from the displacements:

$$\{\varepsilon\} = \{\varepsilon_m\} + \{\varepsilon_p\} = \begin{Bmatrix} \frac{\partial u_0}{\partial x_1} \\ \frac{\partial v_0}{\partial x_2} \\ \frac{\partial u_0}{\partial x_2} + \frac{\partial v_0}{\partial x_1} \end{Bmatrix} - x_3 \begin{Bmatrix} \frac{\partial^2 w_0}{\partial x_1^2} \\ \frac{\partial^2 w_0}{\partial x_2^2} \\ 2 \frac{\partial^2 w_0}{\partial x_1 \partial x_2} \end{Bmatrix} \quad (2.26)$$

where index  $m$  corresponds to the membrane effect and the index  $p$  indicates the plate effect. Equation 2.26 relates the strain field to the displacement field, which may be related to the nodal displacements using the element shape functions. Using these functions and Eq. 2.26, it is possible to relate strains with the DOFs of the finite element as follows:

$$\{\varepsilon\} = [B] \begin{Bmatrix} \mathbf{u}_1 \\ \mathbf{u}_2 \\ \mathbf{u}_3 \end{Bmatrix} \quad (2.27)$$

It is also necessary to relate strains with stresses. For linear elasticity this may be done using a matrix  $[D]$  which is obtained from Hooke's law:

$$\{\sigma\} = [D] \{\varepsilon\} \quad (2.28)$$

In the end, the stiffness matrix of the element is obtained by integrating the domain  $\Omega$  of the element:

$$[K] = \int_{\Omega} [B]^T [D] [B] d\Omega \quad (2.29)$$

More detail about the membrane and plate effects of this element may be consulted in Refs. [3, 4], respectively.

All finite element contributions, including piles and the raft, are assembled to the same system of equations. This system has the form of Eq. 2.23, which is later used to demonstrate how the FEM/BEM coupling is made. The starting point is Eq. 2.21, which may be rewritten as:

$$[H] \{u\} = [T] \{y\} \quad (2.30)$$

Matrix  $[T]$  contains the terms of matrices  $[G]$  and  $[M]$  and  $\{y\}$  contains the distributed loads of vectors  $\{p\}$  and  $\{s\}$ . Next step is isolating the distributed loads, which are transformed in nodal loads using a matrix  $[Q]$ .

$$[T]^{-1} [H] \{u\} = \{y\} \rightarrow [B] \{u\} = \{y\} \quad (2.31)$$

$$[Q] [B] \{u\} = [Q] \{y\} \rightarrow [D] \{u\} = \{r\} \quad (2.32)$$

Before relating Eqs. 2.23 and 2.32, they must be expanded as to contain all degrees of freedom defined in the coupled FEM-BEM model. The result is

$$[\bar{K}] \{\bar{u}_{FEM}\} = \{\bar{f}\} - \{\bar{r}_{FEM}\}, \quad [\bar{D}] \{\bar{u}_{BEM}\} = \{\bar{r}_{BEM}\} \quad (2.33)$$

These equations are related by imposing compatibility and equilibrium conditions, which are  $\{\bar{u}_{FEM}\} = \{\bar{u}_{BEM}\} = \{\bar{u}\}$  and  $\{\bar{r}_{FEM}\} = \{\bar{r}_{BEM}\} = \{\bar{r}\}$ . The following expression is then obtained:

$$[\bar{K}] \{\bar{u}\} = \{\bar{f}\} - [\bar{D}] \{\bar{u}\} \rightarrow ([\bar{K}] - [\bar{D}]) \{\bar{u}\} = \{\bar{f}\} \rightarrow [\bar{A}] \{\bar{u}\} = \{\bar{f}\} \quad (2.34)$$

where  $\{\bar{u}\}$  contain all unknown displacements of the FEM-BEM model. Once the number of equations is equal to the number of unknowns, the system may be solved obtaining all unknowns.

## 6 Examples

### 6.1 Raft on a Layered Domain

Here a squared raft over a domain with four layers is considered, as presented in Fig. 2.5 with all geometrical and material parameters. Young's module and Poisson ratio are named  $E$  and  $\nu$ , respectively, while thickness is indicated as  $t$ . The subscript  $R$  is used for the raft and numbers are used for the layers. Point  $A$  is at the center of the raft, point  $B$  is at the side midpoint and an uniform 0,1 MPa load is applied over it.

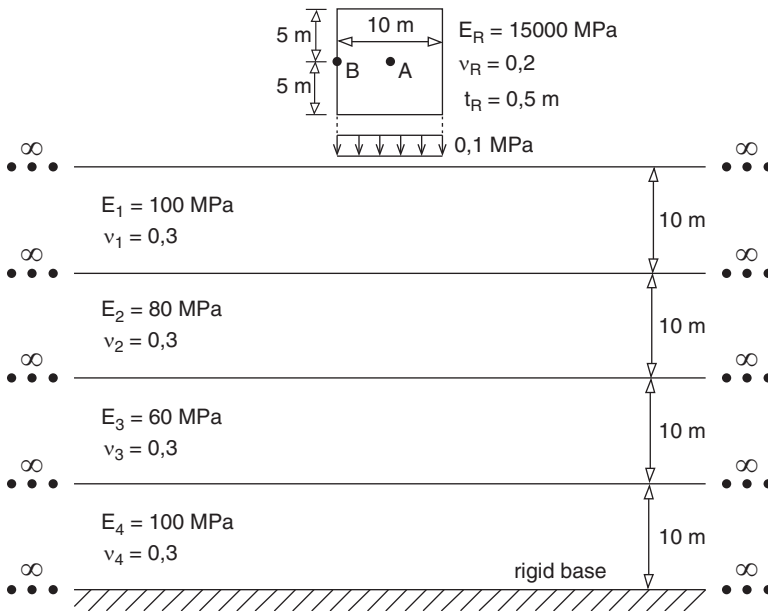
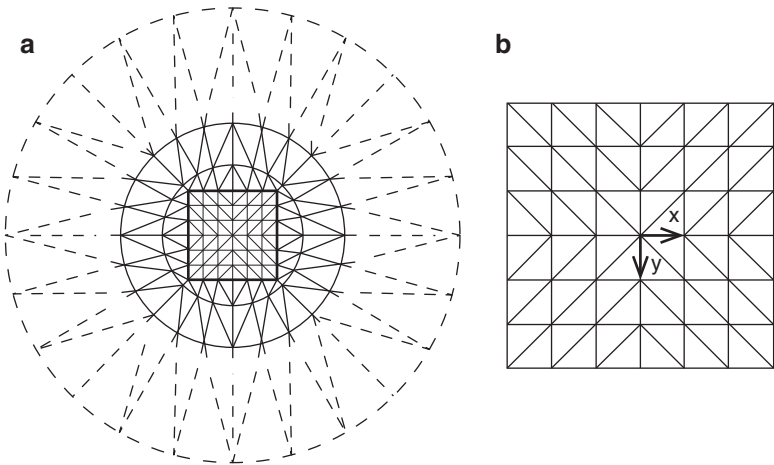


Fig. 2.5 First example



**Fig. 2.6** Mesh employed: (a) soil surface, (b) raft

**Table 2.1** Vertical displacements

	$d_A$ (cm)	$d_B$ (cm)
This work	0,97	0,74
[18]	1,07	0,78
[8]	1,14	0,87
[17]	1,20	0,89

Figure 2.6 presents the mesh. The mesh for the surface and contacts between layers is presented in Fig. 2.6a, where dashed lines represent 48 IBEs and other ones represent 168 BEs. Figure 2.6b presents the 72 FE mesh employed for the raft with an  $xy$  system of coordinates.

Displacements obtained for points  $A$  and  $B$  are presented in Table 2.1 with results obtained by other authors. Good agreement may be observed. To complement this example, the bending moment for axis  $x$  was calculated. The values obtained for points  $A$  and  $B$  were, respectively,  $3,83 \times 10^{-2}$  kNm/m and  $2,20 \times 10^{-2}$  kNm/m.

**6.2 Building Resting on a Layered Domain**

The objective of this example is to demonstrate the generality of the presented formulation. The problem to be analyzed is presented in Fig. 2.7 and considers a building with its foundations, resting on a layered media. In Fig. 2.7a the lateral view is illustrated, Fig. 2.7b contains the standard floor considered and in Fig. 2.7c is presented the top view of the structural foundations included.

The Poisson Ratio is zero for all soil layers. The elasticity modulus of the layers is 60 MPa for the top one, 80 MPa for the second and 90,000 MPa for the base layer.

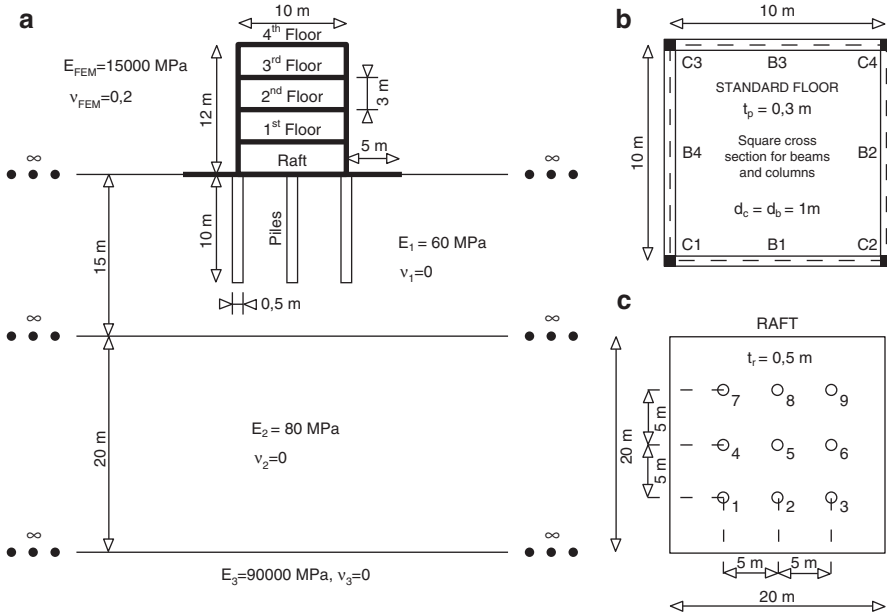


**Fig. 2.7** Soil-building interaction: (a) vertical cut, (b) standard floor, (c) raft

The thickness is 15 m for the top layer, 20 m for the second and the base layer is considered infinite. The diameter of all piles is 0,5 m, their length is 10 m and they are spaced of 5 m. The square raft has size 20 m and thickness 0,5 m. The elasticity modulus of all materials modeled with the FEM is 15,000 MPa and their Poisson ratio is 0,2. This includes all piles, beams, columns, slabs and the raft.

The building has four floors, as shown in Fig. 2.7a. All floors have the same standard geometry, as presented in Fig. 2.7b, with a slab with thickness 0,3 m, four beams supporting this slab and four columns supporting the beams. A cross section  $1 \times 1 \text{ m}^2$  is used for all beams and columns. The base of each column is connected to the raft at the same node where a corner pile is connected. Corner piles are numerated in Fig. 2.7c as 1, 3, 7 and 9.

The loads considered are vertical and presented in Fig. 2.8. They are uniformly distributed over the slabs, with an intensity of 0,04 MPa.

Figure 2.9 presents the FE-BE-IBE mesh employed in the example. Figure 2.9a contains the top view of the mesh used for the soil surface and contacts between layers, totalizing 480 BEs and 96 IBEs. The square detached at the center indicates the position of the raft at the surface. In Fig. 2.9b is illustrated the mesh with 32 FEs used for the raft, together with the position of the piles. Finally, Fig. 2.9c contains the 32 FE mesh used for the slabs. Lines detached at the boundary indicate the FEs used for beams, totalizing 16 FEs for each floor. Furthermore, each part of the columns between floors is divided into 4 FEs. Considering all floors plus the raft,

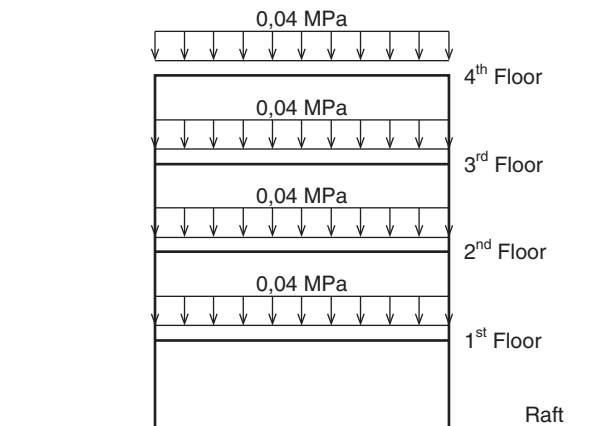


**Fig. 2.8** Vertical loads applied

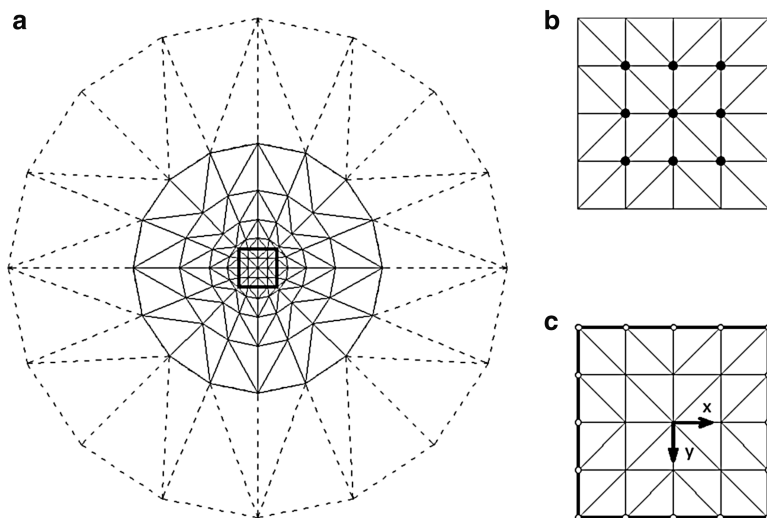


**Fig. 2.9** FE/BE/IBE mesh employed: (a) soil surface, (b) raft, (c) standard floor

the total number of two-dimensional FEs is 160 and the total of one-dimensional FEs is 128.

Piles are also simulated with the FEM, employing the FE with 14 parameters presented previously. The axis of any pile is orthogonal to the surface of the soil.

The vertical displacements along the axis of the piles are shown in Fig. 2.10. Only piles number 1, 2 and 5 are presented (see Fig. 2.7c) because the results are symmetric for the other ones. Piles placed at corners presented higher displacements, with the value of 12,2 mm at the top. This result may be considered coherent because the base of the columns of the building is placed exactly over the corner piles. The

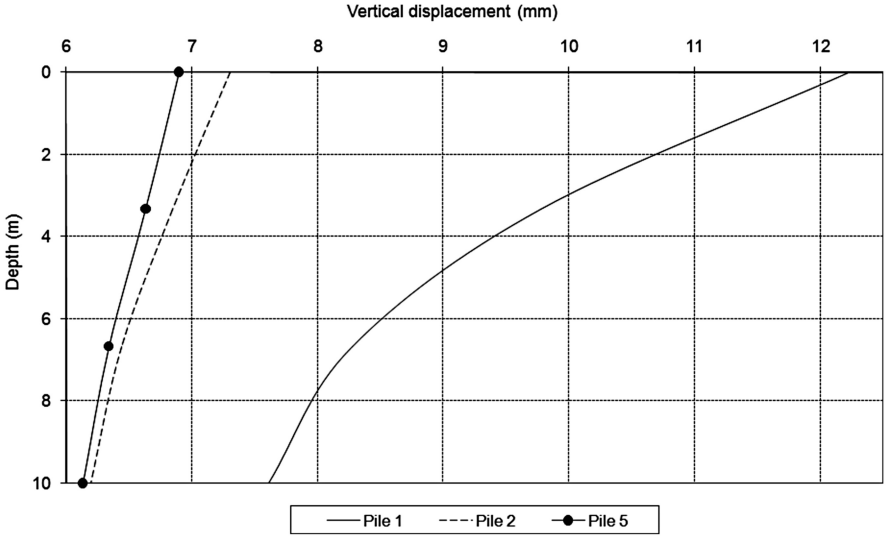


Fig. 2.10 Vertical displacement at slabs

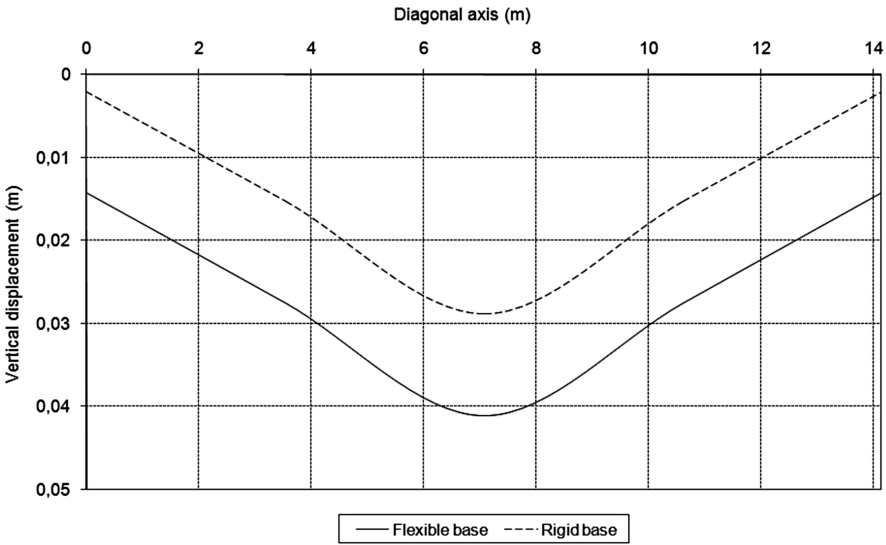


Fig. 2.11 Vertical displacement at the fourth floor

vertical displacement obtained at the top of pile 2 was 7, 3 mm and for pile 5 it was 6, 9 mm.

Figure 2.11 contains results calculated for the fourth floor, as numbered in Fig. 2.7a. Values are evaluated along a diagonal line on the floor, which extremes are placed at columns C1 and C4, as shown in Fig. 2.7b. Two results are presented.

One is considering the elastic foundation presented in Fig. 2.7a and the other is considering a rigid base. For the rigid base, displacements at the base of the columns are simply restrained. It may be observed that the vertical displacements of the slab are significantly higher when an elastic base is considered, what may be considered a predictable result. The maximum displacement at the slab for a rigid base is 28, 8 mm and for an elastic foundation it is 41, 0 mm.

## 7 Conclusions

In this paper a formulation for building-soil interaction analysis was presented. The FEM/BEM equations together with the techniques from Refs. [13, 14] contributed with reducing the total number of degrees of freedom. Piles are modeled using one-dimensional FEs, whose influence in the soil is computed by integrating load lines. Two examples were presented. On the first one the values obtained were compared with other publications and good agreement was observed. On the second one no comparison was presented, nevertheless the results obtained were considered coherent. In the end, it may be concluded that the presented formulation is a powerful and attractive alternative for soil-structure interaction analysis.

**Acknowledgements** Thanks are due to the research council FAPESP, the University of São Paulo and the Federal Institute of São Paulo.

## References

1. Ai, Z.Y., Cheng, Y.C.: Analysis of vertically loaded piles in multi-layered transversely isotropic soils by BEM. *Eng. Anal. Bound Elem.* **37**, 327–335 (2013)
2. Basu, D., Prezzi, M., Salgado, R., Chakraborty, T.: Settlement analysis of piles with rectangular cross sections in multi-layered soils. *Comput. Geotech.* **35**, 563–575 (2008)
3. Batoz, J.L.: A study of tree-node triangular plate bending elements. *Int. J. Numer. Methods Eng.* **15**, 1771–1812 (1980)
4. Bergan, P.G., Felippa, C.A.: A triangular membrane element with rotational degrees of freedom. *Comput. Methods Appl. Mech. Eng.* **50**, 25–69 (1985)
5. Bourgeois, E., de Buhan, P., Hassen, G.: Settlement analysis of piled-raft foundations by means of a multiphase model accounting for soil-pile interactions. *Comput. Geotech.* **46**, 26–38 (2012)
6. Clouteau, D., Cottureau, R., Lombaert, G.: Dynamics of structures coupled with elastic media – a review of numerical models and methods. *J. Sound Vib.* **332**, 2415–2436 (2013)
7. Elahi, H., Moradi, M., Poulos, H.G., Ghalandarzadeh, A.: Pseudostatic approach for seismic analysis of pile group. *Comput. Geotech.* **37**, 25–39 (2010)
8. Fraser, R.A., Wardle, L.J.: Numerical analysis of rectangular rafts on layered foundations. *Geotechnique* **26**, 613–630 (1976)
9. Georgiadis, K., Georgiadis, M., Anagnostopoulos, C.: Lateral bearing capacity of rigid piles near clay slopes. *Soils Found.* **53**, 144–154 (2013)



10. Guiggiani, M., Gigante, A.: A general algorithm for multidimensional cauchy principal value integrals in the boundary element method. *J. Appl. Mech.* **57**, 906–915 (1990)
11. Moser, W., Duenser, C., Beer, G.: Mapped infinite elements for three-dimensional multi-region boundary element analysis. *Int. J. Numer. Methods Eng.* **61**, 317–328 (2004)
12. Padron, L.A., Aznarez, J.J., Maeso, O.: 3-D boundary element-finite element method for the dynamic analysis of piled buildings. *Eng. Anal. Bound. Elem.* **35**, 465–477 (2011)
13. Ribeiro, D.B., Paiva, J.B.: An alternative multi-region BEM technique for three-dimensional elastic problems. *Eng. Anal. Bound. Elem.* **33**, 499–507 (2009)
14. Ribeiro, D.B., Paiva, J.B.: Analyzing static three-dimensional elastic domains with a new infinite boundary element formulation. *Eng. Anal. Bound. Elem.* **34**, 707–713 (2010)
15. Ribeiro, D.B., Paiva, J.B.: Mixed FEM-BEM formulations applied to soil-structure interaction problems. In: *Proceedings of the World Congress on Engineering 2014 (WCE 2014)*, London, 2–4 July 2014. *Lecture Notes in Engineering and Computer Science*, pp. 1178–1183 (2014)
16. Su, D., Li, J.H.: Three-dimensional finite element study of a single pile response to multidirectional lateral loadings incorporating the simplified state-dependent dilatancy model. *Comput. Geotech.* **50**, 129–142 (2013)
17. Wang, Y.H., Tham, L.G., Tsui, Y., Yue, Z.Q.: Plate on layered foundation analyzed by a semi-analytical and semi-numerical method. *Comput. Geotech.* **30**, 409–418 (2003)
18. Wardle, L.J., Fraser, R.A.: Finite element analysis of a plate on a layered cross-anisotropic foundation. In: *Proceedings of the First International Conference of Finite Element Methods in Engineering*, University of New South Wales, pp. 565–578 (1974)

Transactions on Engineering Technologies

World Congress on Engineering 2014

Yang, G.-C.; Ao, S.-I.; Gelman, L. (Eds.)

2015, XI, 773 p. 353 illus., 205 illus. in color., Hardcover

ISBN: 978-94-017-9803-7